

# Mysteries of supercooled water elucidated by studies of aqueous solutions

Peter Lunkenheimer<sup>1</sup>✉, Daniel Reuter<sup>1</sup>, Arthur Schulz<sup>1</sup>, Martin Wolf<sup>1</sup> & Alois Loidl<sup>1</sup>

<sup>1</sup> Experimental Physics V, Center for Electronic Correlations and Magnetism, University of Augsburg, 86135 Augsburg, Germany

✉ e-mail: peter.lunkenheimer@physik.uni-augsburg.de

The most abundant form of water in the universe probably is its supercooled state, staying non-crystalline down to lowest temperatures. The many peculiarities of liquid water, like its partly negative thermal expansion, have been traced back to prominent anomalies occurring in its supercooled form – especially under elevated pressure – and to the presence of two variants of supercooled water and of amorphous, glassy ice. However, the bare existence of these different liquid states and of a related liquid-liquid crossover at ambient pressure are controversially debated since decades, just as the absolute value of water's glass-transition temperature. Their direct experimental detection is hampered by the inevitable crystallization of pure water in a certain temperature range, termed "no-man's land". To tackle these problems, we have applied dielectric spectroscopy and differential scanning calorimetry to aqueous LiCl solutions. By covering a frequency range of up to 14 decades and by quenching some of the solutions to avoid crystallization, here we show that there are indeed strong hints at two forms of water, occurring in different temperature ranges and having different glass-transition temperatures, even at ambient pressure: A so-called "fragile" liquid, characterized by super-Arrhenius temperature dependence of the molecular dynamics at high temperatures, and a "strong" liquid, nearly following Arrhenius behaviour, at low temperatures.

Water is anomalous in many respects, e.g., it expands on cooling just before crystallizing, is denser than ice and exhibits a very complex  $p,T$  phase diagram.<sup>1</sup> Many of these properties can be explained assuming two forms of water, mirroring the existence of polyamorphous ice at lower temperatures<sup>2,3,4</sup>. As function of temperature and pressure, they are separated by a first-order liquid-liquid phase-transition and a phase-coexistence line, suggested to end at a second critical point at about 220 K and 100 MPa.<sup>1,2,4,5,6</sup> At lower pressures and higher temperatures, the phase-separation line is continued by the Widom line, which may explain a suggested<sup>7,8</sup> crossover from so-called fragile water at high, into strong water at low temperatures<sup>1,9,10</sup>

Molecular dynamics can be quantified by the relaxation time  $\tau$ . Within the strong-fragile classification system<sup>11</sup>, its typical deviations from thermally activated Arrhenius temperature-dependence are well-pronounced in "fragile" liquids but weak in "strong" ones. These deviations are thought to arise from the cooperativity of molecular motions<sup>12</sup> and can be quantified by the fragility index  $m$  (Supplementary Note 1)<sup>13</sup>. Water's possible fragile-strong transition (FST) and its glass transition are controversial<sup>1,3,10,14,15,16,17,18,19,20</sup> because both are hidden within the no-man's land (NML)<sup>2</sup>, between about 150 and 235 K, where crystallization prevents their direct experimental detection. In contrast, such transitions are well established for a number of other materials revealing tetrahedral coordination like liquid silica<sup>2,10,11,21</sup>. To detect the FST of water, several strategies were explored to avoid crystallization: Admixing salts or other compounds<sup>4,14,16,22,23,24,25,26,27,28,29</sup>, confining water in nanoscopic geometries<sup>30,31,32,33</sup> or investigating bound water, e.g., in protein hydration shells<sup>34,35,36</sup>. In all cases, concerns may be raised about the relevance of the obtained results for pure bulk water. Interestingly, various computer experiments suggest two liquid forms of water<sup>2,5,6,37</sup>. Nevertheless, the fact that even the bare existence of fragile water and a FST is doubted by many scientists<sup>15,20,35,38,39,40,41,42</sup>, although it was proposed more than 20 years ago, demonstrates the lack of clear experimental

evidence until now. As stated in Ref. 39, "we can conclude so far there is no experimental confirmation of the existence of the strong-fragile transition".

Here we investigate aqueous LiCl solutions with salt concentrations  $x = 1.8\text{--}7.3$  mol%, guided by comments from Angell<sup>14,24</sup> that, for such low salt contents, indeed an FST should be observable. By performing extreme broadband dielectric measurements, extending to THz frequencies, complemented by DSC experiments, and by quenching low-concentration samples to prevent crystallization, we shed new light on the FST in pure water. While aqueous LiCl solutions have been investigated previously<sup>14,16,22,23,24,26,27,29</sup>, all these earlier works suffered from the restriction to high salt concentrations or from partial crystallization. In the present work, for the first time we succeeded in supercooling solutions with relatively low LiCl contents. This enables much more significant conclusions on the FST of water and even allowed for the direct detection of such a transition at the lowest concentration.

Aqueous solutions with  $x \gtrsim 10$  mol% can be easily supercooled without crystallization, i.e., they do not reveal an NML<sup>26,43</sup>. As an example, Fig. 1a shows spectra of the dielectric loss  $\epsilon''$  for  $x = 14.8$  mol% at various temperatures<sup>28</sup>. Here, the inevitable contribution from the dc-conductivity  $\sigma_{dc}$  was subtracted to illustrate the molecular relaxation behaviour (Supplementary Note 2). The latter leads to a loss peak ascribable to the structural  $\alpha$  relaxation<sup>28</sup>. As shown in Ref. 28, upon addition of LiCl this peak smoothly develops from the main loss peak of water, located at room temperature at about 20 GHz. It should be noted that in some works this peak is analysed in terms of the sum of several Debye functions<sup>44,45,46</sup>. As we detect a single peak only, following Occam's razor, we refrain from such an analysis, which can be quite arbitrary. This is discussed in some detail in Ref. 28. It should also be noted that, in the solutions, part of the water molecules should reside in hydration shells around the ions for time scales of  $10^{-11}$  s<sup>47</sup>. Anyway, our spectra (including those in the supercooled quenched samples

treated below) reveal no trace of a possible separate relaxation process due to hydration water.

such high salt concentrations make it questionable whether the results are of significance for pure water<sup>33</sup>.

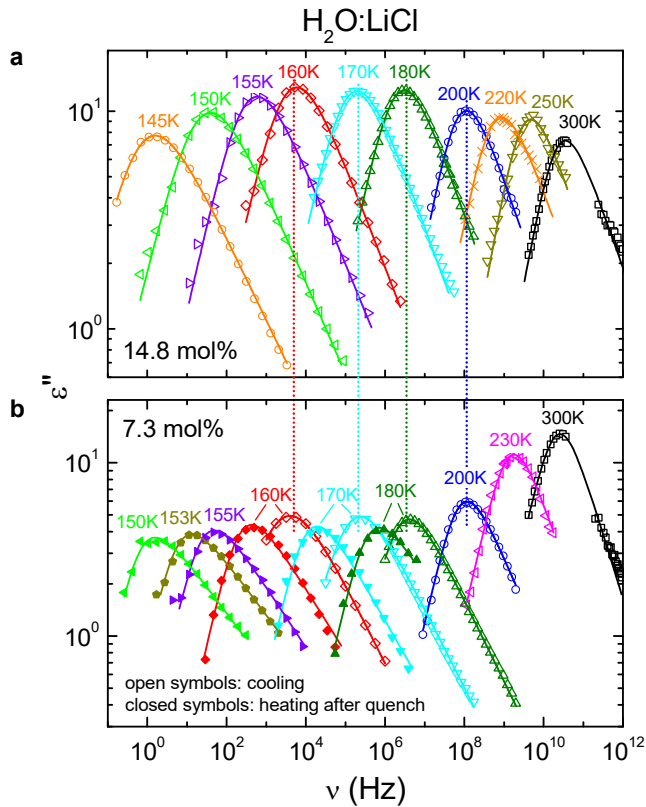


**Fig. 1 | Dielectric-loss spectra of aqueous LiCl solutions after correction for dc conductivity.** The loss  $\epsilon''(\nu)$  is shown using double-logarithmic scales for selected temperatures. **a** Loss spectra of the 14.8 mol% solution, taken from ref. 28 (here we omitted the high-frequency contributions treated in that work). At this high salt concentration, crystallization does not occur even for small cooling rates. **b** Spectra of the 7.3 mol% solution. The data shown by open symbols were determined on cooling with moderate rates of order 0.5 K/min. Upon cooling, the sample partially crystallizes and the data at  $T \leq 200$  K essentially reflect the behaviour of the liquid pentahydrate fraction (16.7 mol%; Supplementary Note 3). The closed symbols show results measured upon heating after the sample was rapidly quenched in liquid nitrogen. They characterize the dynamics of the homogeneous supercooled-liquid state. The solid lines in **(a)** and **(b)** are fits with the empirical Havriliak-Negami and Cole-Davidson function, respectively. The dotted vertical lines demonstrate the approximate agreement of the peak positions in the phase-separated 7.3 mol% sample (whose liquid fraction has about 16.7 mol% LiCl content) with those of the 14.8 mol% sample.

The many-decades shift of the peak frequency  $\nu_p \approx 1/(2\pi\tau)$  to lower frequencies upon cooling, revealed in Fig. 1a, mirrors the tremendous continuous slowing down of molecular dynamics when approaching the glass transition. The open circles in Fig. 2 show an Arrhenius plot of  $\tau(T)$  deduced from these data. It extends from the picosecond range in the low-viscosity liquid, deep into the highly viscous supercooled-liquid regime, thereby crossing water's NML (blue-shaded area). The red line in Fig. 2 is a fit of  $\tau(T)$  by the empirical Vogel-Fulcher-Tammann (VFT) law (Supplementary Note 1), commonly employed to parameterize relaxation-time data in glass-forming liquids<sup>11,12,13</sup>. It reasonably describes the experimental data without any indication of an FST. Similar conclusions were drawn from dielectric measurements below 3 GHz of a 12 mol% solution<sup>26</sup>. However,

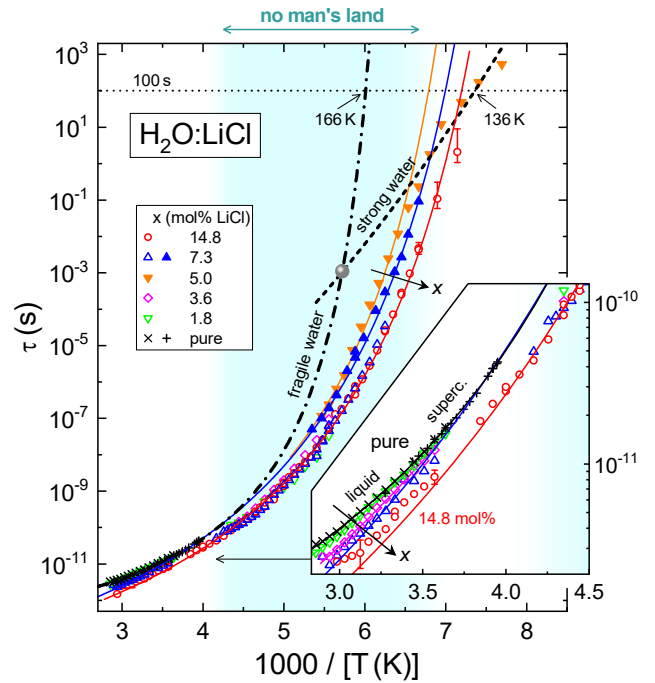


**Fig. 2 | Temperature dependence of the mean relaxation times.** The figure shows an Arrhenius representation of  $\tau(T)$  of pure water and of aqueous LiCl solutions as resulting from fits of the dielectric spectra. The NML of water is indicated by the blue shaded region. The inset presents an enlarged view of the relaxation times at high temperatures. The open symbols denote relaxation times deduced from the broadband dielectric experiments using conventional heating and cooling rates. Those measured on the quenched samples with 7.3 and 5.0 mol% are shown by the closed triangles up and down, respectively. The crosses and pluses illustrate  $\tau(T)$  of pure water at temperatures above the NML<sup>28,48</sup>. The solid lines are VFT fits for the solutions. The dash-dotted line represents the VFT fit to the results obtained for liquid and supercooled pure water at high temperatures (crosses and pluses), i.e., for the fragile form of water. The dashed line is an estimated VFT law for the suggested strong form of water, calculated from the extrapolated values of  $T_g$  and  $m$  for  $x \rightarrow 0$  (Fig. 3, dashed lines). The grey sphere indicates the estimated FST of pure water. The dotted horizontal line at  $\tau = 100$  s represents the typical relaxation time at the glass-transition temperature.

Therefore, we performed measurements at lower concentrations between 1.8 and 7.3 mol%. However, even for 7.3 mol%, partial crystallization occurs, i.e., a NML also exists for such solutions, at least for moderate cooling rates. This is, e.g., revealed by the dielectric measurements as demonstrated for 7.3 mol% in Fig. 1b: The open symbols show the conductivity-corrected loss peaks, detected using cooling rates of the order 0.5 K/min. We have fitted the raw dielectric spectra, simultaneously accounting for the dielectric-constant spectra,  $\epsilon'(\nu)$ , as described in Supplementary Note 2. This leads to the  $\tau(T)$  values shown by the open upright triangles in Fig. 2. There, data for pure liquid and supercooled water at high temperatures, outside the NML, are also included (crosses: determined from the spectra in ref. 28; pluses: from ref. 48). As seen in the inset, at high temperatures the data for 7.3 mol% lie between those for pure water and 14.8 mol% (open circles), which is reasonable. However, at lower temperatures, within the NML,  $\tau(T)$  for 7.3 mol% LiCl agrees with the results for 14.8 mol% within experimental resolution. This also becomes obvious in Fig. 1,

where the dotted lines demonstrate virtually identical peak positions for identical temperatures for both concentrations in this temperature range. For the 1.8 and 3.6 mol% samples, we found similar behaviour: a systematic variation of  $\tau(x)$  at high temperatures, outside the NML, but an agreement with  $\tau$  of the 14.8 mol% sample within it.

The detection of relaxation processes at low temperatures in the 1.8–7.3 mol% samples excludes their complete crystallization, in contrast to pure water within the NML. In fact, they undergo phase separation, i.e., only part of the sample crystallizes into ice upon cooling (Supplementary Note 3). As the salt ions are not incorporated into the ice fraction, the remaining liquid fraction becomes enriched in LiCl concentration during this process. It stops when a stable salt concentration of about 16.7 mol% (pentahydrate; LiCl:5H<sub>2</sub>O) is reached. Thus, the dielectric data in the NML for these low-concentration solutions essentially reflect the behaviour of their liquid fraction with ~16.7 mol% LiCl. This explains why their  $\tau(T)$  is nearly identical to that of the similar concentration of 14.8 mol% within the NML (Fig. 2). Partial crystallization also explains the significant reduction of the loss-peak amplitude, observed when crossing over into the NML upon moderate cooling (Fig. 1b, open symbols). Overall, from such dielectric measurements no conclusions can be drawn concerning possible FSTs in low-concentrated LiCl solutions or pure water.

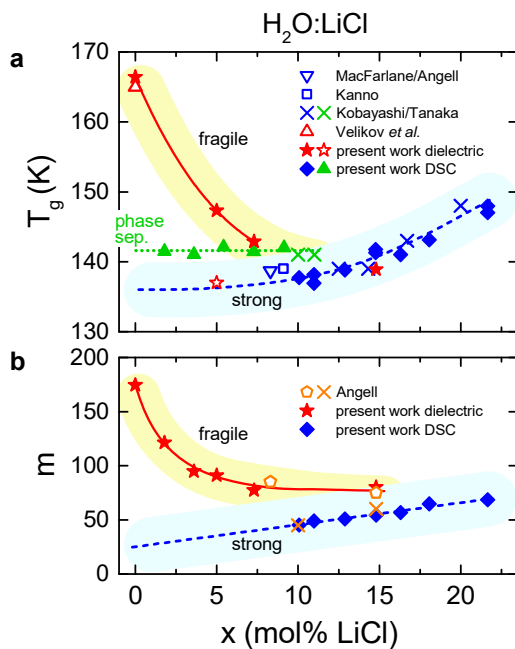


**Fig. 3 | Concentration dependence of glass-transition temperature and fragility.** **a** Glass-transition temperatures  $T_g$  and, **b**, fragility indices  $m$  as observed in aqueous LiCl solutions. All lines are drawn to guide the eye. The closed diamonds and closed triangles show the present results from DSC experiments (see Supplementary Note 4). The  $T_g(x)$  results in (a) are complemented by literature data from MacFarlane and Angell<sup>51</sup>, Kanno<sup>50</sup> and Kobayashi/Tanaka<sup>49</sup> as indicated in the figure legend. The green symbols denote results for phase-separated samples. The blue symbols were determined for homogeneous samples around the glass temperature, in the supposed strong water state. The red stars show results determined from the dielectric relaxation times (Fig. 2) of homogeneous samples, including pure water and the quenched samples at 5 and 7.3 mol%, as described in the text. The upright open triangle in (a) indicates the glass-transition temperature of pure water proposed by Velikov et al.<sup>57</sup>. In (b), additional  $m(x)$  data for the strong and fragile states of LiCl solutions, taken from ref. 14, are included (pentagons and crosses).

This phase-separation scenario is also confirmed by DSC measurements that we performed for solutions with  $x = 1.8$ –21.7 mol% (Supplementary Note 4). Figure 3a shows the resulting glass-transition temperatures (closed diamonds and triangles). For  $x \geq 10$  mol% (diamonds),  $T_g$  exhibits a weak but significant increase with increasing LiCl content, in agreement with earlier results<sup>22,49,50,51</sup> (partly included in the figure). However, for lower salt concentrations (closed triangles),  $T_g(x)$  is essentially constant, consistent with literature data for 10 and 11 mol% (green crosses)<sup>49</sup>. Its value of ~142 K corresponds to that of a homogeneous solution of about 16–17 mol%. This also points to partial crystallization giving rise to the formation of a liquid pentahydrate phase for all concentrations below 10 mol%. Interestingly, an extrapolation of the glass-transition temperatures at  $x > 10\%$  to low concentrations (dashed line) is consistent with a  $T_g$  of 136 K, lying within the range often assumed for pure water<sup>38,52,53,54,55</sup> (however, see ref. 23 for a more complex  $T_g(x)$  behaviour of hyperquenched solutions, nevertheless leading to a similar  $T_g(x \rightarrow 0)$ ).

We also performed DSC measurements with different heating/cooling rates to determine the fragility using the method promoted, e.g., in ref. 56 (Supplementary Note 4). The resulting  $m(x)$  (Fig. 3b, diamonds) reveals an approximately linear decrease with decreasing concentration. Such a decrease was also reported in ref. 49 where, however, different  $m$  values were found for different experimental methods. An extrapolation of  $m(x)$  (dashed line) leads to  $m \approx 25$  for pure water, consistent with the notion that deeply supercooled water is a strong liquid<sup>7,30,55</sup>.

Using  $m = 25$  and  $T_g = 136$  K from the above-discussed extrapolations (dashed lines in Fig. 3), and assuming  $\tau_0 = 10^{-14}$  s as a standard value for the inverse attempt frequency<sup>13</sup>, we arrive at a rough estimate for  $\tau(T)$  of strong water as shown by the dashed line in Fig. 2. It clearly does not match the high-temperature experimental data of liquid and supercooled water without assuming an anomaly. Similar conclusions from comparisons of pure-water dynamics measured at temperatures above and below the NML were drawn previously<sup>7,8,24,42</sup>.

Although low-concentration LiCl solutions, cooled with moderate rates, crystallize and phase separate at low temperatures, for them the inaccessibility of the NML may be less strict than for pure water. Indeed, at least for the samples with 5 and 7.3 mol%, we were able to avoid any crystallization and phase separation by quenching them in liquid nitrogen. Typical results measured upon heating after the quench are shown for 7.3 mol% by the closed symbols in Fig. 1a. For 160, 170 and 180 K, the quenched and phase-separated samples reveal significantly different peak positions. Moreover, in contrast to the latter, the peak frequencies for the quenched sample do not agree with those of the 14.8 mol% sample (Fig. 1a), speaking against phase separation. Similar findings were obtained for the quenched 5% solution. Fitting the raw dielectric spectra of both quenched solutions (Supplementary Note 2), leads to  $\tau(T)$  as shown by the closed upright and inverted triangles in Fig. 2. In contrast to the phase-separated samples, within the NML,  $\tau$  of these quenched solutions systematically increases with decreasing salt content, confirming that phase separation, accompanied by the formation of a pentahydrate liquid fraction, plays no role here. This systematic development (including the homogeneous 14.8 mol% sample) indicates that the relaxation time of pure water within the NML should be even higher.

The lines through these data points are fits with the VFT formula. (As for 5 mol% no high-temperature data were measured, the pre-exponential factor  $\tau_0$  was fixed to an interpolated value, based on fit results for the other concentrations.) The mentioned increase of  $\tau$  with decreasing  $x$  essentially can be traced back to an increase of the glass-

transition temperature (139, 143 and 147 K for  $x = 14.8, 7.3$  and 5%, respectively) which can be estimated from the VFT parameters using the condition  $\tau(T_g) \approx 100$  s. The dash-dotted line in Fig. 2 shows a VFT fit of the pure-water  $\tau(T)$  data at high temperatures<sup>28,48</sup> (crosses and plusses in Fig. 2; see also Fig. 4). It leads to even higher  $T_g$  of 166 K. This value has an uncertainty of about 15 K (Supplementary Note 5) as it is essentially based on an extrapolation of the VFT fit of the low-viscosity-liquid data up to 100 s. Nevertheless, it reasonably matches with the  $T_g(x)$  trend revealed by the solutions (closed stars in Fig. 3a) and with the glass-transition temperatures reported in literature for water above the NML<sup>57,58</sup>.

From the obtained VFT fit parameters, the fragility index  $m$  can be derived (Supplementary Note 1)<sup>13</sup>. For pure water, we find it to be extremely high ( $m \sim 175$  K 175). Very high fragility of water above the NML was also reported, based on thermodynamic measurements<sup>8,57</sup> and on viscosity data<sup>59</sup> covering a similar temperature range as the pure-water  $\tau(T)$  data in Fig. 2. The latter are partly based on detailed permittivity measurements up to 20 THz<sup>28</sup>. In contrast to previous works, these spectra include the real part of the permittivity and the low- and high-frequency flanks of the loss peaks, determined at different temperatures. Therefore, the resulting  $\tau(T)$  data are of unprecedented precision. Notably, they cannot be well fitted when fixing  $m$  to values below about 100 and they are incompatible with  $T_g = 136$  K (Fig. 4; see also Supplementary Note 5). The obtained fragility indices of pure water and of the solutions are shown by the closed stars in Fig. 3b. Here we also include data for 1.8 and 3.6 mol%, for which experimental data in the homogeneous state are only available in a rather small temperature range at high temperatures (inset of Fig. 2). Thus, we have fitted them using fixed values for  $T_{VF}$ , obtained by interpolation. Again, a continuous trend of  $m(x)$  of the solutions is revealed, well consistent with the deduced high fragility of pure water.

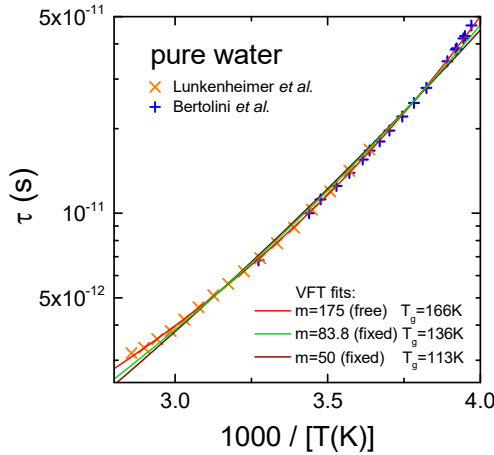


**Fig. 4 | Relaxation time of pure water.** Arrhenius representation of  $\tau(T)$  at temperatures above the NML (plusses: from Ref. 48; crosses: derived from the high-frequency dielectric spectra published in ref. 28). The lines are VFT fits with different fragility indices  $m$  (partly fixed) and different resulting values of  $T_g$  as indicated in the legend (see Supplementary Note 5 for more details).

As indicated by the sphere in Fig. 2, an extrapolation of the VFT fit of the high-temperature water data crosses the above-mentioned estimate of  $\tau(T)$  of strong water (dash-dotted line), derived from the  $x \rightarrow 0$  extrapolations shown by the dashed lines

in Fig. 3. This crossing occurs at 175 K, which represents a rough estimate of the FST temperature of water, based on the present results (of course, the actual crossover probably is more smeared out<sup>14,42</sup>). In literature, values in the range of 190 - 228 K were reported<sup>4,8,16,18,31</sup>. The deduced FST temperature of 175 K has some uncertainty, e.g., because the dashed line is based on the extrapolations in Fig. 3 (dashed lines). Therefore, the behaviour of pure water within the NML, indicated in Fig. 2, should be regarded as one possible, most simple scenario only, and here we do not aim at a precise prediction of  $\tau(T)$  within the NML. Nevertheless, one should note that the dash-dotted line in Fig. 2 is based on  $\tau(T)$  data of unprecedented precision as discussed above. Even if neglecting the dashed line, the VFT curve shown by the dash-dotted line (or corresponding lines with lower or higher  $T_g$  within the given error of 15 K; see Supplementary Fig. 7) does not smoothly match the Arrhenius behaviour of deeply supercooled liquid water, reported at temperatures below the no-man's land<sup>1,55</sup>. Therefore, somewhere in the NML,  $\tau(T)$  must start to deviate from the well-defined VFT behaviour detected at higher temperatures, i.e., an FST must occur (see Supplementary Note 5 for more details). Based on the pure-water data, we cannot say whether  $\tau(T)$  exhibits an abrupt or more smeared-out change of slope. As discussed below, in the quenched 5 mol% LiCl solution, the latter is found.

Figure 3 reveals that, for the homogeneous low-concentration LiCl solutions, both  $T_g$  and  $m$  markedly increase with decreasing salt content (closed stars). This *increase* strongly contrasts with the *decrease* of both quantities found for the high-concentration solutions (closed diamonds). For the fragility, these opposite trends were previously pointed out by Angell<sup>14</sup>, based on sparse viscosity and DSC data only (pentagons and crosses in Fig. 3b, respectively) and interpreted as indicative of an FST of pure water. For 14.8 mol% the values of  $T_g$  from the dielectric and DSC experiments are in accord and  $m$  does not differ dramatically. In contrast,  $m(x)$  and  $T_g(x)$  at lower concentrations clearly do not agree with the extrapolated behaviour of the samples with  $x > 10$  mol% (dashed lines in Fig. 3). That is, an extrapolation to  $x = 0$  of the dielectric (or viscosity<sup>14</sup>) data leads to markedly different properties of pure water than an extrapolation of the DSC results. To understand this apparent discrepancy, one should note that the latter are based on measurements at low temperatures, around  $T_g$ . In contrast, the analysis of the dielectric experiments is based on results above  $T_g$ , mostly even extending far into the low-viscosity liquid range. For 14.8 mol%, both methods lead to comparable results but for low salt contents this is not the case. Therefore, we conclude that, at high concentrations, there is essentially only a single state of these water solutions, persisting at all temperatures<sup>26</sup>. The extrapolation of its properties to pure water is in accord with the strong state of pure water with  $T_g \approx 136$  K as deduced from low-temperature data on hyperquenched or pressure-driven amorphous water<sup>1,52,53,54</sup>. However, for the low-concentration solutions and pure water, an additional fragile state exists at high temperatures. Its  $T_g(x)$  and  $m(x)$  significantly increase for decreasing salt contents, but at high concentrations merge with the results from the low-temperature measurements. As indicated by the solid lines in Fig. 3, this increase is in full accord with  $T_g \approx 166$  K and with the high fragility of 175 obtained from the VFT fit of pure water.

If indeed two states of water exist, a transition between them should occur upon temperature variation. For pure water it is unobservable due to the NML and only can be estimated (sphere in Fig. 2). Can it be observed in the investigated quenched solutions that allow exploring this region? As seen in Fig. 2, just as for 14.8 mol%,  $\tau(1/T)$  for 7.3 mol% does not reveal any anomaly up to tau values of about 0.1 s, which corresponds to

loss-peak frequencies of the order of 1 Hz. However, for the 5 mol% solution we have extended the dielectric measurements to frequencies down to 100  $\mu$ Hz (Supplementary Fig. 1). This enables the detection of a crossover of  $\tau(1/T)$  into a significantly weaker temperature variation at low temperatures, characteristic of a stronger liquid. Using  $\tau(T_g) \approx 100$  s, we arrive at a glass-transition temperature of 137 K for this strong state of the solution. As shown by the open star in Fig. 3a, it is in good accord with the extrapolated  $T_g(x)$  curve of the strong high- $x$  solutions. This is another confirmation that an FST occurs in low-concentration LiCl solutions and, thus, also in pure water. Interestingly, the largest  $\tau$  value for the 14.8 mol% sample in Fig. 2 also slightly deviates from the VFT fit, which may indicate an FST even for this sample, in accord with the somewhat different fragilities from the dielectric and DSC measurements (Fig. 3b).

In summary, from our measurements of water and of LiCl solutions, we have obtained strong hints at two forms of pure water separated by an FST. While other investigations of aqueous solutions usually rely on extrapolations to  $x=0$  to uncover the properties of pure water, we want to point out that our conclusions are largely independent of such extrapolations. In particular, they are based on the following achievements: (i) The unprecedented precision of our  $\tau(T)$  data for pure water at high temperatures, proving its high fragility and excluding a match to low-temperature data of water without an FST. (ii) The direct detection of an FST for a quenched low-concentration sample, to our knowledge never achieved before in an aqueous solution. While high-concentration solutions lack such a transition, its emergence at low concentrations clearly points to its existence in pure water, too. (iii) The contradicting  $T_g(x)$  and  $m(x)$  behaviour detected (without extrapolation) by dielectric spectroscopy at high and by DSC at low temperatures, pointing to two forms of water, depending on temperature. Again, the emergence of this phenomenon at low concentrations, while it is absent at high ones, makes it implausible that it should be absent in pure water. For our estimate of the pure-water behaviour in the NML shown in Fig. 2 and of the transition temperature of 175 K, extrapolations indeed play a major role, but these estimates are not essential for the conclusions of the present work.

This experimentally documented existence of two forms of water at high and low temperatures with different glass-transition temperatures answers the very controversial question regarding the occurrence of fragile water and the FST. Moreover, it helps to solve the controversy on  $T_g$  of water: The commonly accepted  $T_g$  of 136 K refers to the strong form of water which persists at low temperatures and, thus, is the true glass-transition temperature. The value of 166 K characterizes the fragile liquid and supercooled-liquid form of water at high temperatures. However, below a temperature  $T_{FST} > 166$  K (roughly estimated here to be  $\sim 175$  K), it undergoes an FST before glassy freezing at 166 K can occur, shifting the glass transition to 136 K. Notably, a  $T_g$  of 136 K is only compatible with the high-temperature water data when assuming an FST, i.e.,  $T_g \approx 136$  K implies an FST and vice versa.

Our findings will allow for the comparison of theoretical and computer-simulation-based interpretations of the FST with a highly improved data basis compared to published work. An example is the interpretation by Shi et al. (Ref. 42), which assumes a transition between two strong liquids instead of an FST. As our  $\tau(T)$  data extend to significantly larger temperatures than the diffusion data analysed by Shi et al., we are able to prove in our manuscript that water at high temperatures is a fragile liquid, and by no means follows Arrhenius behaviour (see, e.g., Fig. 4). We think, checking whether or not our results are compatible with this or other models, will stimulate further

advance in the understanding of supercooled water and of its FST.

## Methods

### Samples

The samples were prepared by diluting an aqueous 8 mol/l LiCl solution (Sigma Aldrich) with deionized H<sub>2</sub>O (Merck "Ultrapure"). Higher concentrated solutions were made by mixing deionized H<sub>2</sub>O with pure LiCl salt (ChemPur) which was stored and weighed in argon atmosphere to prevent water absorption. Concentrations are given in mol%. Please note that in a previous publication<sup>28</sup> we specified the number (percentage) of LiCl molecules per one water molecule. In the present work, we use mol% LiCl to be compatible with published work treating concentration-dependent data.

### Dielectric measurements

For dielectric spectroscopy, a combination of several techniques was used: At frequencies up to 1 MHz, we employed a frequency-response analyser (Novocontrol "Alpha-A" analyser). In the interval from 1 MHz to 3 GHz, a coaxial reflectometric setup including impedance analysers (Agilent 4294A and Agilent E4991A) was used. In both cases, the samples were put into parallel-plate capacitors. The frequency range from 100 MHz to 40 GHz was covered by a coaxial open-end reflection technique, using the Agilent "Dielectric Probe Kit" and the Agilent E8363B Network Analyzer. For the highest frequencies up to about 1 THz, a terahertz time-domain spectrometer TPS Spectra 3000 by Teraview Ltd. was used. More information about the measurement principals and setups can be found in ref. 28 and references therein.

For cooling, a N<sub>2</sub> gas cryostat (Novocontrol Quatro) with home-made insets, a helium-flow cryostat and Peltier elements were used. For quenching, performed in the gas cryostat at frequencies up to 3 MHz, the complete cryostat inset, including the wired and filled sample capacitor, was first immersed into liquid nitrogen before putting it into the precooled cryostat. The achieved cooling rate was too fast to be properly monitored. In earlier DSC measurements<sup>22,23,29</sup>, aqueous LiCl solutions with  $x < 9$  mol% were found to be impossible to supercool by liquid-nitrogen quenching. Probably the achieved cooling rates were higher and/or the sample environment (capacitors with polished stainless-steel plates in N<sub>2</sub> atmosphere) favoured the avoidance of crystallization in the present experiments.

### Differential scanning calorimetry

DSC measurements were performed with a DSC 8500 (Perkin Elmer). The device was calibrated for heating measurement runs with a 3-point method using n-dodecane, n-heptane and indium as standard samples. For the measurements, small amounts of sample material (< 20 mg) were hermetically sealed into aluminium pans. To determine  $m$ , the measurement procedure was adapted from Wang et al.<sup>56</sup> The "standard scan rate" was set to 10 K/min and the cooling rate was varied between 0.5 and 100 K/min.

### Data availability

The data that support the findings of this study are available from the corresponding author upon reasonable request.

### Acknowledgements

We thank M. Schwab for performing part of the dielectric measurements beyond GHz.

## Author contributions

A.L. and P.L. initiated this work. D.R., A.S. and M.W. collected and analysed the experimental data. P.L. analysed the data and prepared the figures. A.L. and P.L. wrote the manuscript. All authors discussed the results and commented on the manuscript.

## Competing interests

The authors declare no competing interests.

## Additional information

Supplementary Information is available for this paper.

Correspondence and requests for materials should be addressed to Peter Lunkenheimer.

Reprints and permissions information is available at [www.nature.com/reprints](http://www.nature.com/reprints).

## References

1. Amann-Winkel, K. et al. Colloquium: Water's controversial glass transitions. *Rev. Mod. Phys.* **88**, 011002 (2016).
2. Mishima, H. & Stanley, H. E. The relationship between liquid, supercooled and glassy water. *Nature* **396**, 329–335 (1998).
3. Debenedetti, P. G. Supercooled and glassy water. *J. Phys.: Condens. Matter* **15**, R1669–R1726 (2003).
4. Woutersen, S., Ensig, B., Hilbers, M., Zhao, Z. & Angell, C. A. A liquid-liquid transition in supercooled aqueous solution related to the HDA-LDA transition. *Science* **359**, 1127–1131 (2018).
5. Poole, P. H., Sciortino, F., Essmann, U. & Stanley, H. E. Phase behaviour of metastable water. *Nature* **360**, 324–328 (1992).
6. Debenedetti, P. G., Scortino, F. & Zerze G. H. Second critical point in two realistic models of water. *Science* **369**, 289–292 (2020).
7. Angell, C. A. Water II is a "strong" liquid. *J. Phys. Chem.* **97**, 6339–6341 (1993).
8. Ito, K., Moynihan, C. T. & Angell, C. A. Thermodynamic determination of fragility in liquids and a fragile-to-strong liquid transition in water. *Nature* **398**, 492–495 (1999).
9. Xu, L. et al. Relation between the Widom line and the dynamic crossover in systems with a liquid-liquid phase transition. *Proc. Natl. Acad. Sci. USA* **102**, 16558–16562 (2005).
10. Gallo, P. et al. Water: A tale of two liquids. *Chem. Rev.* **116**, 7463–7500 (2016).
11. Angell, C. A. Formation of glasses from liquids and biopolymers. *Science* **267**, 1924–1935 (1995).
12. Debenedetti, P. G. & Stillinger, F. H. Supercooled liquids and the glass transition. *Nature* **410**, 259–267 (2001).
13. Böhmer, R., Ngai, K. L., Angell, C. A. & Plazek, D. J. Nonexponential relaxations in strong and fragile glass formers. *J. Chem. Phys.* **99**, 4201–4209 (1993).
14. Angell, C. A. Liquid fragility and the glass transition in water and aqueous solutions. *Chem. Rev.* **102**, 2627–2650 (2002).
15. Johari, G. P. Does water need a new  $T_g$ ? *J. Chem. Phys.* **116**, 8067–8873 (2002).
16. Angell, C. A. Insights into phases of liquid water from study of its unusual glass-forming properties. *Science* **319**, 582–587 (2008).
17. Palmer, J. C. et al. Metastable liquid-liquid transition in a molecular model of water. *Nature* **510**, 385–388 (2014).
18. Kim, K. H. et al. Experimental observation of the liquid-liquid transition in bulk supercooled water under pressure. *Science* **370**, 978–982 (2020).
19. Kringle, L., Thornley, W. A., Kay, B. D. & Kimmel, G. A. Reversible structural transformations in supercooled liquid water from 135 to 245 K. *Science* **369**, 1490–1492 (2020).
20. Krüger, C. R., Mowry, N. J., Bongiovanni, G., Drabbels, M. & Lorenz, U. J. Electron diffraction of deeply supercooled water in no man's land. *Nat. Commun.* **14**, 2812 (2023).
21. Saika-Voivod, I., Poole, P. H. & Sciortino, F. Fragile-to-strong transition and polymorphism in the energy landscape of liquid silica. *Nature* **412**, 514–517 (2001).
22. Angell, C. A. & Sare, E. J. Glass forming composition regions and glass transition temperatures for aqueous electrolyte solutions. *J. Chem. Phys.* **52**, 1058–1068 (1970).
23. Hofer, K., Hallbrucker, A., Mayer, E. & Johari, G. P. Vitrified dilute aqueous-solutions. 3. Plasticization of water's H-bonded network and the glass-transition temperature's minimum. *J. Phys. Chem.* **93**, 4674–4677 (1989).
24. Angell, C. A. et al. Liquid fragility and the glass transition in water and aqueous solutions. *Int. J. Food Sci.* **22**, 115–142 (1994).
25. Murata, K. & Tanaka, H. Liquid-liquid transition without macroscopic phase separation in a water-glycerol mixture. *Nature Mater.* **11**, 436–443 (2012).
26. Nakanishi, M., Griffin, P., Mamontov, E. & Sokolov, A. P. No fragile-to-strong crossover in LiCl-H<sub>2</sub>O solution. *J. Chem. Phys.* **136**, 124512 (2012).
27. Münzer, P., Hoffmann, L., Böhmer, R. & Gainaru, C. Deeply supercooled aqueous LiCl solution studied by frequency-resolved shear rheology. *J. Chem Phys.* **150**, 234505 (2019).
28. Lunkenheimer, P. et al. Electromagnetic-radiation absorption by water. *Phys. Rev. E* **96**, 062607 (2017).
29. Bachler, J., Handle, P. H., Giovambattista, N. & Loerting, T. Glass polymorphism and liquid-liquid phase transition in aqueous solutions: Experiments and computer simulations. *Phys. Chem. Chem. Phys.* **21**, 23238–23268 (2019).
30. Bergman, R. & Swenson, J. Dynamics of supercooled water in confined geometry. *Nature* **403**, 283 (2000).
31. Faraone, A., Liu, L., Mou, C.-Y., Yen, C.-W. & Chen, S.-H. Fragile-to-strong liquid transition in deeply supercooled confined water. *J. Chem. Phys.* **121**, 10843 (2004).
32. Fischer, J. K. et al. Supercooled water confined in a metal-organic framework. *Commun. Phys.* **3**, 95 (2020).
33. Cervený, S., Mallamace, F., Swenson, J., Vogel, M. & Xu, L. Confined water as model of supercooled water. *Chem. Rev.* **116**, 7608–7625 (2016).
34. Chen, S.-H. et al. Observation of fragile-to-strong dynamic crossover in protein hydration water. *Proc. Natl. Acad. Sci. USA*, **103**, 9012–9016 (2006).
35. Doster, W. et al. Dynamical transition of protein-hydration water. *Phys. Rev. Lett.* **104**, 098101 (2010).
36. Wolf, M., Emmert, S., Gulich, R., Lunkenheimer, P. & Loidl, A. Dynamics of protein hydration water. *Phys. Rev. E* **92**, 032727 (2015).
37. Gartner, T. E., Piaggi, P. M., Car, R., Panagiotopoulos, A. Z. & Debenedetti, P. G. Liquid-liquid transition in water from first principles. *Phys. Rev. Lett.* **129**, 255702 (2022).
38. Johari, G. P., Tombari, E., Salvetti, G. & Mallamace, F. Does water need a  $\lambda$ -type transition? *J. Chem. Phys.* **130**, 126102 (2009).
39. Capaccioli, S. & Ngai, K. L. Resolving the controversy on the glass transition temperature of water? *J. Chem. Phys.* **135**, 104504 (2011).
40. Swenson, J. Comment on "Pressure Dependence of Fragile-to-Strong Transition and a Possible Second Critical Point in Supercooled Confined Water". *Phys. Rev. Lett.* **97**, 189801 (2006).
41. Cervený, S., Alegria, A. & Colmenero, J. Comment on "Pressure Dependence of Fragile-to-Strong Transition and a Possible Second Critical Point in Supercooled Confined Water". *Phys. Rev. Lett.* **97**, 189802 (2006).
42. Shi, R., Russo, J. & Tanaka, H. Origin of the emergent fragile-to-strong transition in supercooled water. *Proc. Natl. Acad. Sci. USA* **115**, 9444–9449 (2018).

- 
43. Kobayashi M. & Tanaka H. Possible link of the V-shaped phase diagram to the glass-forming ability and fragility in a water-salt mixture. *Phys. Rev. Lett.* **106**, 125703 (2011).
  44. Kaatze, U., Behrends, R. & Pottel, R. Hydrogen network fluctuations and dielectric spectrometry of liquids. *J. Non-Cryst. Solids* **305**, 19 (2002).
  45. Yada, H., Nagai, M. & Tanaka, K. Origin of the fast relaxation component of water and heavy water revealed by terahertz time-domain attenuated total reflection spectroscopy, *Chem. Phys. Lett.* **464**, 166 (2008).
  46. Arbe, A., Malo de Molina, P., Alvarez, F., Frick, B. & Colmenero, J. Dielectric susceptibility of liquid water: microscopic insights from coherent and incoherent neutron scattering. *Phys. Rev. Lett.* **117**, 185501 (2016).
  47. Mason, P. E., Ansell, S., Neilson, G. W. & Rempe, S. B. Neutron scattering studies of the hydration structure of Li<sup>+</sup>. *J. Phys. Chem. B* **119**, 2003–2009 (2015).
  48. Bertolini, D., Cassettari, M. & Salvetti, G. The dielectric relaxation time of supercooled water. *J. Chem. Phys.* **76**, 3285 (1982).
  49. Kobayashi, M. & Tanaka, H., Relationship between the phase diagram, the glass-forming ability, and the fragility of a water/salt mixture. *J. Phys. Chem. B* **115**, 14077–14090 (2011).
  50. Kanno, H. Double glass transitions in aqueous lithium chloride solutions vitrified at high pressures: Evidence for a liquid-liquid immiscibility. *J. Phys. Chem.* **91**, 1967–1971 (1987).
  51. MacFarlane, D. R. & Angell, C. A. Nonexistent glass transition for amorphous solid water. *J. Phys. Chem.* **88**, 759–762 (1984).
  52. McMillan, J. A. & Los, S. C. Vitreous ice: Irreversible transformations during warm-up. *Nature* **206**, 806–807 (1965).
  53. Johari, G. P., Hallbrucker, A. & Mayer, E. The glass-liquid transition of hyperquenched water. *Nature* **330**, 552–553 (1987).
  54. Hallbrucker, A., Mayer E. & Johari, G. P. Glass-liquid transition and the enthalpy of devitrification of annealed vapor-deposited amorphous solid water. A comparison with hyperquenched glassy water. *J. Phys. Chem.* **93**, 4986 (1989).
  55. Amann-Winkel K. et al. Water's second glass transition. *Proc. Natl. Acad. Sci. USA* **110**, 17720–17725 (2013).
  56. Wang, L.-M., Velikov, V. & Angell, C. A. Direct determination of kinetic fragility indices of glassforming liquids by differential scanning calorimetry: Kinetic versus thermodynamic fragilities. *J. Chem. Phys.* **117**, 10184 (2002).
  57. Velikov, V., Borick, S. & Angell, C. A. The glass transition of water, based on hyperquenching experiments. *Science* **294**, 2335–2338 (2001).
  58. Cerveny, S., Schwartz, G. A., Bergman, R. & Swenson, J. Glass transition and relaxation processes in supercooled water. *Phys. Rev. Lett.* **93**, 245702 (2004).
  59. Dehaoui, A., Issenmann, B. & Caupin, F. Viscosity of deeply supercooled water and its coupling to molecular diffusion. *Proc. Natl Acad. Sci.* **112**, 12020–12025 (2015).

# Supplementary Information

for

## Mysteries of supercooled water elucidated by studies of aqueous solutions

Peter Lunkenheimer, Daniel Reuter, Arthur Schulz, Martin Wolf & Alois Loidl

Experimental Physics V, Center for Electronic Correlations and Magnetism, University of Augsburg, 86135 Augsburg, Germany

### Contents:

- Supplementary Note 1: VFT law and fragility
- Supplementary Note 2: Fits of permittivity spectra
- Supplementary Note 3: The binary phase diagram of H<sub>2</sub>O:LiCl
- Supplementary Note 4: Dynamic Scanning Calorimetry on H<sub>2</sub>O:LiCl
- Supplementary Note 5: Relaxation time of pure water

### Supplementary Note 1: VFT law and fragility

The temperature dependence of relaxation processes in liquids generally does not follow a simple thermally activated, Arrhenius-type behaviour, but can be often described well utilizing the time-honoured empirical Vogel-Fulcher-Tammann (VFT) law<sup>1</sup>. In a variety of supercooled liquids ranging from strong to fragile glass formers, the VFT law provides a reasonable description of broadband data<sup>2,3,4</sup>. (However, while the VFT still is most commonly applied, one should be aware that also more theoretically founded approaches were proposed to describe  $\tau(T)$ , see, e.g., refs. <sup>5,6</sup>.) In a modified form of the VFT law<sup>4</sup>, the temperature dependence of the mean relaxation time  $\tau$  is given by:

$$\tau = \tau_0 \exp\left(\frac{DT_{VF}}{T-T_{VF}}\right) \quad (1)$$

Here  $\tau_0$  is a prefactor related to the inverse attempt frequency,  $T_{VF}$  is the Vogel-Fulcher temperature, where the relaxation times would diverge in the case of infinitely slow cooling and  $D$  is the strength parameter, which can be used to parameterize the deviations from the Arrhenius law<sup>4</sup>. Alternatively, these deviations can be quantified by the fragility index  $m^{7,8}$ , which represents the steepness of the temperature dependence of the mean relaxation time  $\tau$  in an Angell plot,  $\log \tau$  vs.  $T_g/T$ , exactly at the glass-transition temperature. Thus, the fragility index  $m$  is given by:

$$m = \frac{d \log \tau}{d(T_g/T)} \Big|_{T=T_g} \quad (2)$$

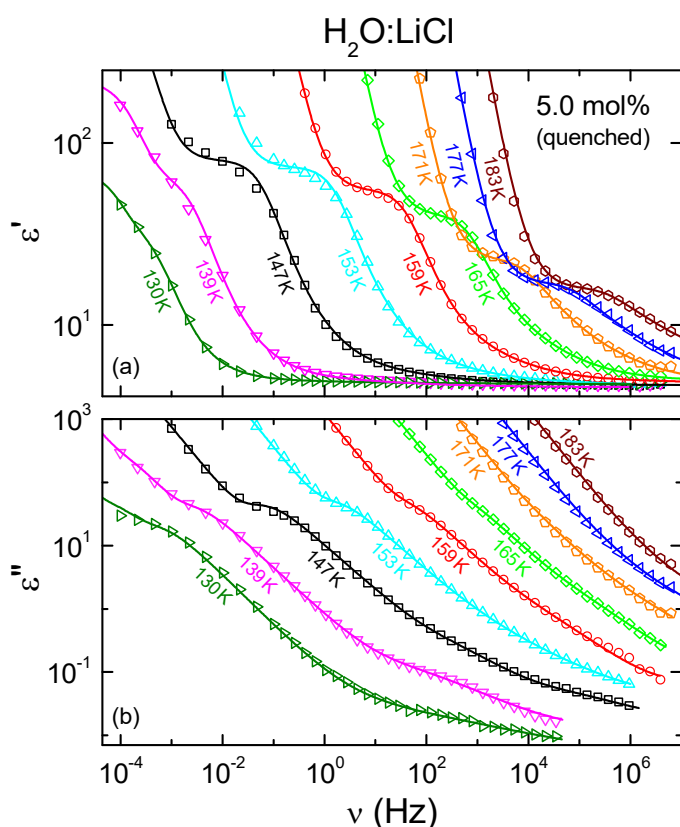
In so-called strong liquids,  $\tau(T)$  only weakly deviates from Arrhenius-type behaviour and  $m = 16$  represents a lower bound of possible values (depending on the choice of  $\tau_0$ )<sup>7</sup>, corresponding to exact Arrhenius behaviour. In fragile liquids,  $\tau(T)$  strongly deviates from an Arrhenius law, indicating super-Arrhenius behaviour, and  $m$  can be larger than 100, but only very rarely exceeds values of 170.<sup>3,9</sup> In case of a perfect VFT behaviour, the fragility index is related to  $D$  via<sup>7</sup>:

$$m = 16 + 590/D \quad (3)$$

### Supplementary Note 2: Fits of the permittivity spectra

Via the common relation  $\varepsilon'' \propto \sigma'/\nu$  (where  $\sigma'$  is the real part of the conductivity), the ionic charge transport in the investigated aqueous LiCl solutions leads to an inevitable contribution to the dielectric loss spectra arising from the ionic dc-conductivity  $\sigma_{dc}$  and dominating at low frequencies. As a typical example, Supplementary Fig. 1b shows the raw  $\varepsilon''$  spectra of the quenched 5 mol% sample. The mentioned dc contribution is revealed by the  $1/\nu$  upturn of  $\varepsilon''(\nu)$  at low

frequencies (not completely shown). At high temperatures, it essentially completely superimposes the expected relaxation peaks related to the reorientational motions of the water molecules while, at low temperatures, these peaks are still evidenced by shoulders in the spectra. In contrast, in  $\epsilon''(\nu)$  (Supplementary Fig. 1a), where there is no contribution from dc charge transport, the sigmoidal steps expected for a dipolar relaxation process are clearly revealed. In the loss spectra shown in Fig. 1 of the main paper, the dc contribution was subtracted to illustrate the molecular relaxation behaviour. However, to avoid ambiguities that may arise from the  $\sigma_{dc}$  subtraction (already a small variation of the subtracted  $\sigma_{dc}$  can change the peak frequency), we have fitted the raw dielectric spectra, including a contribution  $\epsilon''_{dc} = \sigma_{dc}/(2\pi\nu\epsilon_0)$  in the overall fit function ( $\epsilon_0$  denotes the permittivity of vacuum). Moreover, we have also simultaneously fitted the independently measured real part of the permittivity,  $\epsilon'$ , which is not hampered by the dc conductivity. The additional increase of  $\epsilon'(\nu)$  with decreasing frequency, documented at low frequencies in Supplementary Fig. 1a, can be ascribed to electrode polarization, sometimes termed "blocking electrodes". This is a well-known effect for ionic conductors and caused by the accumulation of the ions at the sample-electrode interfaces at low frequencies<sup>10</sup>. In the performed fits, it was taken into account by assuming a parallel RC circuit connected in series to the sample, as described in detail in refs. 10 and 11. To describe the dipolar-relaxation process of the water molecules, the empirical Cole-Davidson function<sup>12</sup>, often employed to fit dielectric spectra of dipolar glass formers<sup>13,14</sup>, was used. Finally, at low temperatures and high frequencies, an excess-wing like contribution<sup>13,14,15</sup> is revealed in the loss spectra of Supplementary Fig. 1b. It was formally taken into account by up to two Cole-Cole functions<sup>16</sup> as often used for secondary relaxation processes<sup>14,17</sup>.

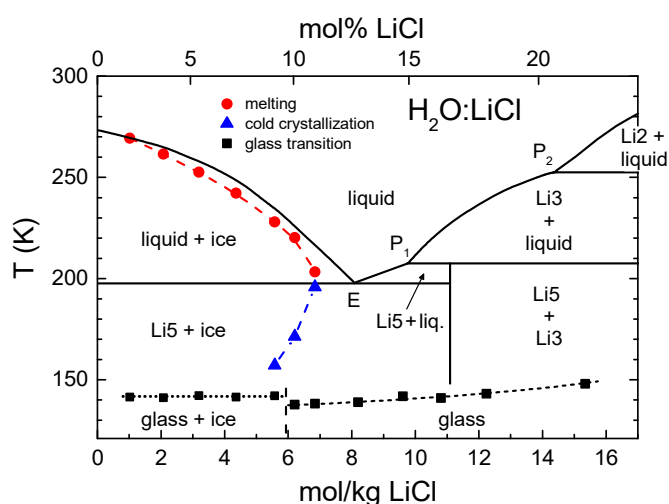


**Supplementary Fig. 1 | Complex permittivity spectra of a quenched aqueous solution with 5.0 mol% LiCl. a** Real part of the dielectric permittivity  $\epsilon'$ . **b** Imaginary part  $\epsilon''$ . For both quantities, raw data, including conductivity contributions and effects of electrode polarization, are shown on double logarithmic scales for various temperatures. The lines indicate fits as discussed in the text.

As shown by the lines in Supplementary Fig. 1, reasonable fits of the experimental data could be achieved in this way. It should be noted that for none of the measured spectra, all the different contributions, discussed above, had to be simultaneously used in the fits. For example, at high temperatures, the excess-wing like feature is not seen and, at low temperatures, electrode effects are absent. We also want to point out that, at all temperatures, a step and point of inflection is detected in the  $\epsilon'$  spectra which clearly restricts the uncertainty of the water relaxation-time obtained from the fits. This is also the case for the results on the quenched 7.3 mol% solution.

### Supplementary Note 3: The binary phase diagram of H<sub>2</sub>O:LiCl

By extensive measurements, as well as by compilation and critical evaluation of literature data, the binary phase diagram of H<sub>2</sub>O:LiCl was established in detail by Monnin et al.,<sup>18</sup> Li et al.<sup>19</sup> and Yim and Abu-Lebdeh.<sup>20</sup> This equilibrium phase diagram shows a characteristic eutectic point at a temperature between 190 and 200 K and at a LiCl concentration of 8 mol/kg(H<sub>2</sub>O), corresponding to approximately 12.6 mol% LiCl (Supplementary Fig. 2). On further increasing salt concentrations, the melting line increases again and exhibits a sequence of peritectic points. In addition to the pure phases, four solid lithium-chloride hydrates, with respectively 1, 2, 3 and 5 water molecules, were identified. In the dilute aqueous limit, the most stable configuration is the pentahydrate LiCl:5H<sub>2</sub>O (Li5), which correspond to a concentration of  $x = 0.167$  mol%. It was established that Li<sup>+</sup> prefers tetrahedral and Cl<sup>-</sup> octahedral oxygen coordination of neighbouring water molecules.<sup>21</sup> Utilizing Raman-scattering techniques, the average hydration number of these Li<sup>+</sup>Cl<sup>-</sup> molecular clusters has been determined to be close to  $R = 5.3$  by Green et al.<sup>22</sup> At lower LiCl concentrations and low temperatures, the pentahydrate coexists with pure hexagonal ice and undergoes complete phase separation, while at higher concentrations regimes of coexisting hydrate crystals were identified. Hence, for concentrations  $x < 0.167$  pentahydrate coexists with pure water ice (Li5 + ice), while for  $x > 0.167$  combinations of various hydrate crystals (e.g., Li5 + Li3) dominate. As observed in many binary systems, at low temperatures the tendency to glass formation is strongly enhanced around the eutectic point. As documented in the course of this work and as reported in literature, in the LiCl:H<sub>2</sub>O system, by conventional cooling methods and cooling rates of bulk systems, glassy low-temperature states can be observed for molar salt concentrations  $10 < x < 25$  mol%.



**Supplementary Fig. 2 | Phase diagram.** Low-concentration equilibrium ( $x, T$ ) phase diagram of H<sub>2</sub>O: LiCl as determined by Monnin et al.<sup>18</sup> Solid lines indicate equilibrium phase boundaries. Li2, Li3 and Li5 denote phases with 2, 3 and 5 water molecules per LiCl. The eutectic point E is at 199 K and 8 mol/kg LiCl (lower abscissa) corresponding to approximately 12.6 mol% LiCl (upper abscissa). Peritectic points  $P_i$  are indicated along the melting line beyond the eutectic point. Full symbols represent results as determined by DSC measurements in the present work: Circles indicate crystallization observed on cooling when entering the two-phase regime and squares show glass-transition temperatures. Depending on the cooling rate, below about 10 mol% a glassy LiCl:5H<sub>2</sub>O phase coexists with crystalline water (see text). Close to the eutectic point, clear evidence for recrystallization of the supercooled liquid fraction on heating was observed (triangles up). Dotted and dashed lines are drawn to guide the eye.

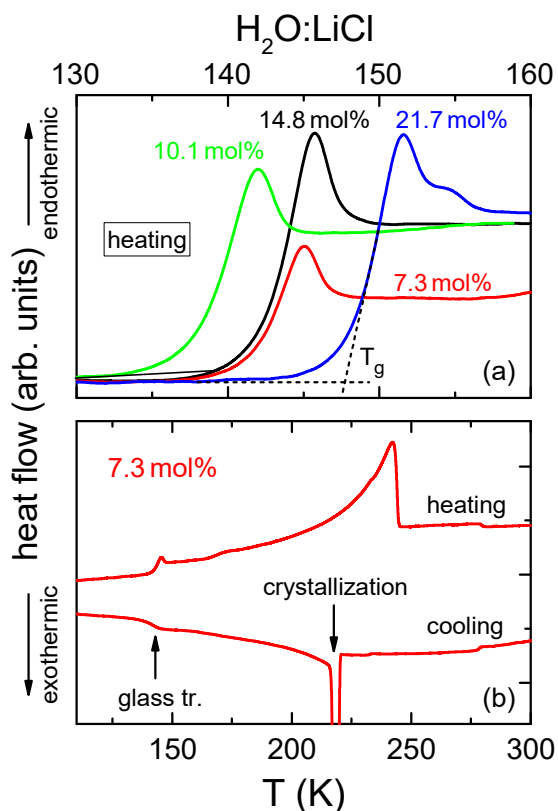
As discussed in Supplementary Note 4, we performed systematic DSC measurements as function of temperature and cooling rate for a series of LiCl concentrations ranging from pure water to aqueous solutions with 21.7 mol% LiCl. Part of the results of our measurements are documented in Supplementary Fig. 2: At molar concentrations  $x > 10$  mol%, the aqueous solutions can be easily supercooled without quenching, and we identified signatures of well-defined glass transitions, whose characteristic temperatures (squares in Supplementary Fig. 2) slightly increase from 137 to 150 K with increasing LiCl concentration as also shown in Fig. 3a of the main paper (diamonds). The aqueous solutions in this concentration regime undergo complete vitrification without any indication of crystallization. Upon cooling with moderate rates of the order 0.5 K/min, solutions with lower LiCl concentrations ( $x < 10$  mol%) undergo crystallization of only a fraction of the sample close to the melting line (circles in Supplementary Fig. 2). This results in a phase-separated state of crystalline water and liquid pentahydrate, LiCl:5H<sub>2</sub>O, corresponding to 16.7 mol% LiCl. Subsequently, at temperatures around 142 K the remaining fraction of the liquid phase exhibits a transition into a glassy state. The transition temperature for  $x < 10$  mol% is independent of the LiCl content because the effective LiCl concentration of the liquid fraction is always 16.7 mol%. All our measurements point towards phase separation in this low-concentration

range,  $x < 10$  mol% LiCl, which in Supplementary Fig. 2 is also indicated by an enhanced glass-transition temperature, compared to that at the critical concentration (cf. closed triangles and diamonds in Fig. 3a of the main text). Indeed, the observed 142 K of glassy freezing come very close to the glass-transition temperature of Li5. The homogeneous glass-forming region, without quenching the sample, extends roughly from 10 mol%, a concentration slightly below the eutectic point, up to about 25 mol% LiCl and, of course, strongly depends on the cooling rate.<sup>23,24</sup> However, there is also published work reporting on a homogenous low-temperature phase in this concentration regime.<sup>25</sup>

Close to the eutectic point  $E$ , recrystallization was detected on heating (triangles in Supplementary Fig. 2), which was subsequently followed by an endothermic melting transition. Recrystallization on heating was previously reported for LiCl-doped water samples with  $x < 0.1$ .<sup>26,27</sup> It is generally assumed that on heating the vitreous liquid partly transforms into cubic ice (see, e.g., ref. 28), while on cooling hexagonal ice is formed. The crystallization into cubic ice in pure supercooled water in most cases appears close to 150 K (onset temperature of crystallization).

#### Supplementary Note 4: Dynamic Scanning Calorimetry on H<sub>2</sub>O:LiCl

Supplementary Fig. 3a documents temperature-dependent scans around the glass transition as measured in DSC experiments in aqueous solutions with 7.3, 10.1, 14.8 and 21.7 mol% LiCl. These experiments were performed under constant heating with scan rates of 10 K/min after precooling with the same rate. The samples with  $x = 14.8$  and 21.7 mol% reveal transitions into homogeneous low-temperature glassy states without any indications of crystallization. In the concentration regime  $x < 10$  mol%, the step height becomes significantly reduced, indicating crystallization of a fraction of the sample. The sample with 7.3 mol% lies deep within the phase-separation regime (see Supplementary Note 3). The strongly reduced step in the heat capacity signals that only part of the supercooled liquid is vitrified, while the rest of the sample undergoes crystallization into pure hexagonal water ice. For this concentration, a complete heating and cooling cycle is documented in Supplementary Fig. 3b. On cooling, we find crystallization and, subsequently, a weak glass transition, while on heating the characteristic glass-transition anomaly is followed by an endothermic melting transition.



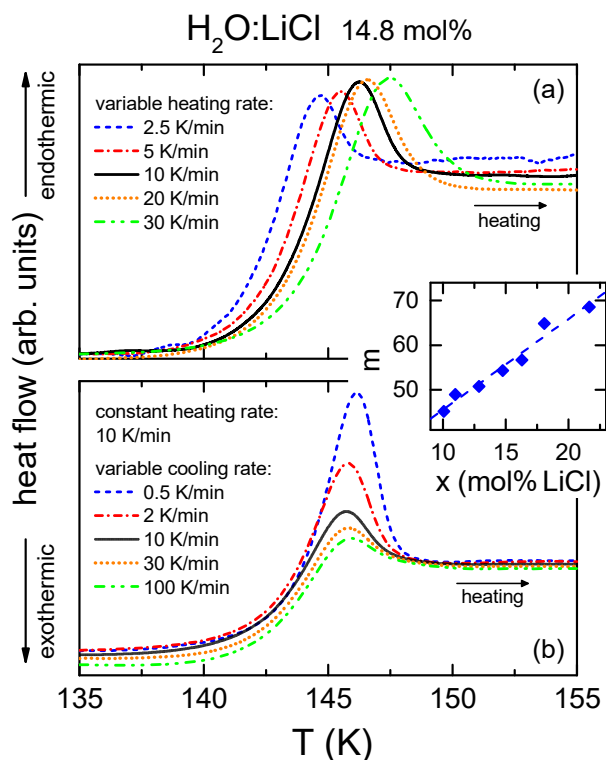
**Supplementary Fig. 3 | DSC results for various LiCl concentrations.** These DSC results were obtained with cooling and heating rates of 10 K/min. **a** Zoom into the glass-transition region of representative samples with 7.3, 10.1, 14.8 and 21.7 mol% measured on heating. Samples with  $x > 10$  mol% exhibit a glass transition, which continuously increases on increasing concentration. The sample with 7.3 mol% reveals an inhomogeneous low-temperature state with coexisting crystalline ice and glassy pentahydrate. The significant reduction in step height signals the reduced glassy volume fraction. The dashed lines for the 21.7 mol% sample indicate the determination of the glass-transition temperature  $T_g$  as the lower onset of the heat-capacity anomaly. **b** A complete cooling and heating cycle in the full temperature range for an aqueous LiCl solution with 7.3 mol%. Glass transition and crystallization or melting, are observed in the heating and cooling cycles, respectively, indicative of phase separation.

Quite often, spectroscopic measurements are performed far above the glass temperature. Thus, the obtained relaxation-time data may be several decades faster than the typical value  $\tau(T_g) \approx 100$  s at glassy freezing. To determine the fragility index  $m$  [eq. (2)],  $\tau(T)$  then has to be extrapolated towards the glass-transition temperature. Similar problems arise for viscosity measurements. Obviously, a method to determine the fragility  $m$  more directly by measuring close to the vitrification temperature seems desirable. Consequently, many efforts were made to determine a liquid's fragility from the heat-flow profile in calorimetric measurements. Pioneering work was published by Moynihan and co-workers,<sup>29,30</sup> introducing the dependence of the glass-transition temperature on the heating and cooling rate to measure the activation energy of the enthalpy relaxation. Later, methods utilizing the evaluation of a single differential thermal analysis<sup>31</sup> or DSC<sup>32</sup> scan were proposed. The success of all these methods depends on the accuracy of these measurements and in addition, how well they can reproduce fragility values obtained from viscosity or relaxation-time measurements. Following this premise, Angell and co-workers<sup>33,34</sup> as well as Yue et al.<sup>35</sup> developed the so-called enthalpy-relaxation method, which reliably can reproduce fragility values in many cases.<sup>34,36</sup>

An alternative approach to directly determine relaxation times and fragility are measurements of the heat-capacity anomaly as function of the heating rate. This method relies on a correlation of heating rate and relaxation times, as determined, e.g., via dielectric spectroscopy. To compare dielectric relaxation times with the DSC fragility data, the Frenkel-Kobeko relation (ref. 37 and references therein) is used:

$$|q| \times \tau(T_g) = C \quad (4)$$

In this equation,  $q$  is the cooling rate,  $\tau(T_g)$  the mean relaxation time at the glass-transition temperature and  $C$  is a constant. In most cases, in literature the glass-transition temperature as observed in DSC measurements using a scanning rate of 10 K/min, is attributed to a mean relaxation time of 100 s.<sup>34,38,39,40</sup> Utilizing this approach leads to  $C = 16.67$  K, which we also adopt in this work. This enables a direct comparison of the temperature dependence of the dielectric relaxation times with the DSC results, which will be discussed below.



**Supplementary Fig. 4 | Glass-transition temperature and fragility investigated by DSC. a** Measurements of a 14.8 mol% LiCl solution with a variable heating rate after cooling with 10 K/min. **b** Application of the enthalpy relaxation method<sup>33,34,35</sup>. The glass transition as recorded during heating with 10 K/min, after cooling the glass with different rates varying between 0.5 and 100 K/min. Inset: Concentration dependence of the fragility index  $m$  determined with the enthalpy relaxation method (same data as shown by the diamonds in Fig. 3b of the main text). The fragilities deduced from the shift of the glass anomaly as documented in (a) give identical results within experimental uncertainties. The dashed line corresponds to a linear fit of the data extrapolating to a value  $m \approx 25$  for pure water.

Supplementary Fig. 4 represents results of the application of both methods to a 14.8 mol% aqueous LiCl solution. In Supplementary Fig. 4a, the solution was cooled with a constant rate of 10 K/min and subsequently heated with variable heating rates between 2.5 and 30 K/min. From these scans, the glass-transition temperatures were determined from the onset of the endothermic heat flow, following the procedure as indicated by the dashed lines in Supplementary Fig. 3a.

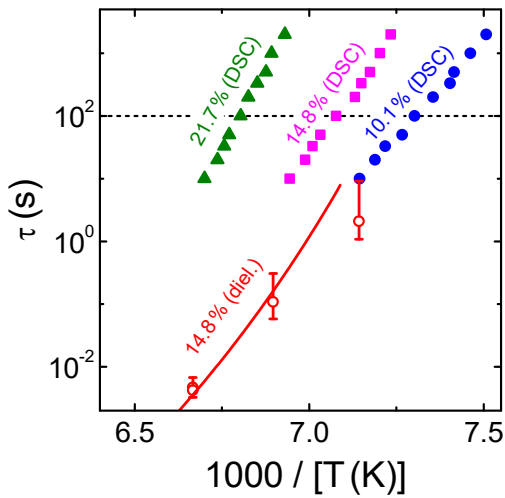
The increasing glass-transition temperature with increasing heating rate is clearly visible. In the present example, for an approximately one-decade increase in heating rate,  $T_g$  changes by about 3 K. Supplementary Fig. 4b documents the enthalpy-relaxation method for the same concentration. In these experiments, the cooling rates were varied between 0.5 and 100 K/min and, subsequently, the sample was heated up with the standard scanning rate of 10 K/min. As can be clearly seen, the shape of the glass transition anomaly recorded during heating strongly depends on the thermal history. Cooling rates slower than the standard one significantly increase the overshoot of the endothermic peak close to 145 K, while faster cooling rates produce a slight decrease of the heat flow preceding the transition step. The cooling-rate dependent enthalpy release  $\Delta H(Q)$  can be determined from the experimental difference between standard scans compared to scans using variable cooling rates. The fictive temperatures  $T_f$  corresponding to the different cooling rates can be calculated using<sup>34</sup>:

$$T_f = T_f^s + \frac{\Delta H(Q)}{\Delta c_p} \quad (5)$$

Here  $T_f^s$  is the fictive temperature, determined from a scan with the standard cooling rate using the method described by Moynihan et al.<sup>29</sup> and  $\Delta c_p$  is the difference in heat capacity between the glass state and the supercooled liquid. Following this procedure,  $m$  can be directly estimated from the slope of the reduced cooling rate  $\log(Q/Q_s)$  versus the inverse reduced fictive temperature  $T_f^s/T_f$ . The inset in Supplementary Fig. 4 shows the concentration dependence of the fragility index  $m$  obtained in this way for a series of aqueous solutions as discussed in detail in the main paper (cf. Fig. 3b, diamonds). We found an almost perfect agreement of the fragility values as determined from both methods described above.

In Supplementary Fig. 5, for the 10.1, 14.8 and 21.7 mol% samples, the closed symbols show an Arrhenius representation of the temperature-dependent relaxation times as deduced via eq. (4) from the rate-dependent DSC measurements discussed above. They span about two decades in  $\tau$  around the calorimetric glass transition. These data enable the determination of the glass-transition temperature by applying the often-used condition  $\tau(T_g) \approx 100$  s, thereby supplementing the direct determination of  $T_g$  from the DSC traces as indicated in Supplementary Fig. 3a. Figure 3a of the main text includes  $T_g$  values from both methods (closed diamonds), which explains the presence of two slightly different values for the 10.1, 14.8 and 21.7 mol% solutions.

For comparison, in Supplementary Fig. 5 we included the results for 14.8 mol% from dielectric spectroscopy as documented in the full temperature range in Fig. 2 of the main text. We find that the slope  $\tau(1/T)$  observed in the dielectric results comes close to that found in the DSC experiments. However, there seems to be a small but significant mismatch of the absolute values of  $\tau$ , which may require a redefinition of the constant  $C$  defined in eq. (4). In Fig. 3a, this small mismatch is mirrored by the difference between the red star and the blue diamond at 14.8 mol%, showing  $T_g$  from the dielectric and DSC measurements. However, as this difference is within the data scatter of the DSC data in Fig. 3a, we consider this issue as unimportant and it does not affect the conclusions of the present work.

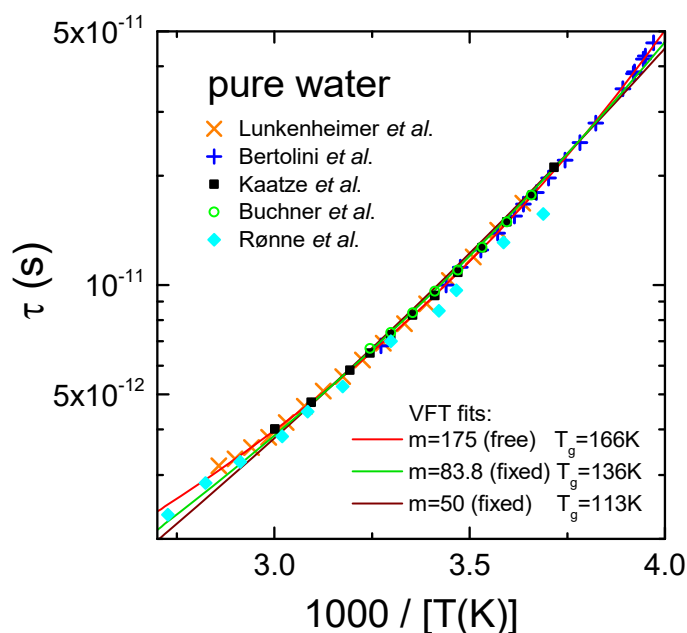


**Supplementary Fig. 5 | Relaxation times from DSC.** The closed symbols show an Arrhenius plot of  $\tau(T)$ , derived from the rate-dependent DSC measurements using eq. (4) with  $C = 16.67$  K, for three salt concentrations. For comparison, the open circles show results as deduced from dielectric spectroscopy in the 14.8 mol% sample in this temperature range. The solid line is a VFT fit [eq. (1)] of the complete  $\tau(T)$  trace of this sample as shown in Fig. 2 of the main paper. The dashed line indicates  $\tau = 100$  s.

## Supplementary Note 5: Relaxation time of pure water

Supplementary Fig. 6 show an Arrhenius plot of the temperature-dependent dielectric relaxation times of pure water. These relaxation-time data were deduced in its liquid and supercooled states at temperatures above the no-man's land (NML). The crosses ( $\times$ ) were determined from the spectra previously reported by Lunkenheimer et al.<sup>41</sup>. We want to point out that, in contrast to other permittivity data on water in literature, the  $\epsilon'$  and  $\epsilon''$  spectra reported in that work, covering about 100 MHz – 20 THz, allow for a detection of the complete relaxation features. This includes the left and right flanks of the loss peaks and the complete steps in  $\epsilon'(\nu)$  at all measured temperatures. This ensures an exceptionally high precision of the deduced  $\tau(T)$  values without having to resort to any assumptions about the spectral shapes or amplitudes of the relaxation features. The  $\tau(T)$  data as reported by Bertolini et al.<sup>42</sup> (plusses) nicely extend those deduced from ref. 41 to lower temperatures. These two data sets agree almost perfectly with those reported in smaller temperature ranges by Kaatze<sup>43</sup> (closed squares) and by Buchner et al.<sup>44</sup> (open circles), also included in Supplementary Fig. 6. Only those by Rønne et al.<sup>45,46</sup> (closed diamonds) somewhat deviate, especially at the lower temperatures, suggesting weaker deviations from Arrhenius behaviour. Thus, we think these data should not be employed for an estimation of the fragility or  $T_g$  of pure water at high temperatures.

In Supplementary Fig. 6, clear deviations of  $\tau(T)$  of water from linear behaviour show up, evidencing non-Arrhenius temperature dependence, typical for glass-forming liquids<sup>2,3,4,7,13,14</sup>. The red line is a VFT fit of the data from refs. 41 and 42 with all parameters free, leading to a very high fragility of  $m = 175$  [calculated from the strength parameter  $D$  in the VFT equation using eq. (3)] and to  $T_g = 166$  K (determined via  $\tau(T_g) \approx 100$  s). The green line is a fit with  $m$  fixed to 83.8, which is adjusted to lead to  $T_g = 136$  K, a value often assumed for water. The deviations of fit and experimental data, however, are significant although  $m$  still is rather large. The brown line, where  $m$  was fixed at a lower value of 50 (intermediate between strong and fragile) demonstrates that the experimental data on pure water above the NML clearly are incompatible with strong dynamics. As mentioned in the main text,  $\tau(T)$  of pure water cannot be reasonably fitted with  $m$  below about 100 and it is clearly incompatible with  $T_g = 136$  K, except when assuming a transition to weaker temperature dependence at lower temperatures.



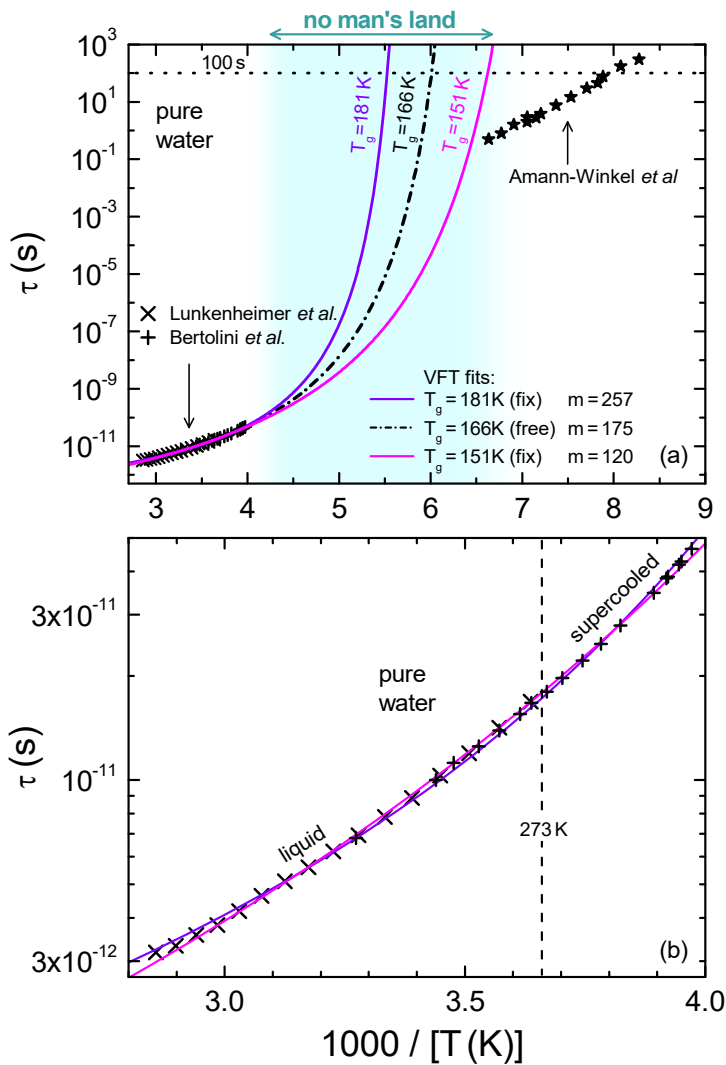
**Supplementary Fig. 6 | Relaxation time of pure water.** Arrhenius representation of  $\tau(T)$  at temperatures above the NML. The lines are VFT fits [eq. (1)] of the data by Bertolini et al.<sup>42</sup> (plusses) and of  $\tau(T)$  derived from the high-frequency dielectric spectra published by Lunkenheimer et al.<sup>41</sup> (crosses). For the fits, different (partly fixed) fragility indices  $m$  were used as indicated in the legend [cf. eq. (3) for the relation between  $m$  and the  $D$  parameter of the VFT equation]. For comparison, also the data from Kaatze et al.<sup>43</sup>, Buchner et al.<sup>44</sup> and Rønne et al.<sup>45,46</sup> are included.

In Supplementary Fig. 7a, we compare  $\tau(T)$  for pure water at temperatures above the NML, derived from refs. 41 and 42, to those for deeply supercooled liquid water (termed "low-density liquid"), reported at temperatures below the NML by Amann-Winkel et al.<sup>47</sup>. The dash-dotted line shows the free VFT fit [eq. (1)] of these data which is the same as the dash-dotted line in Fig. 2 and as the red solid line in Supplementary Fig. 6 and leads to  $T_g \approx 166$  K. Using the commonly assumed condition  $\tau(T_g) \approx 100$  s, from eq. (1) one can derive:

$$T_{VF} = T_g \left[ 1 + \frac{D}{\ln(100s/\tau_0)} \right]^{-1} \quad (6)$$

This allows using  $T_g$  instead of  $T_{VF}$  as a parameter in the VFT fits. Supplementary Fig. 7b shows two VFT fits of the high-temperature water data with  $T_g$  fixed to values that are 15 K higher (violet line) or lower (magenta line) than  $T_g \approx 166$  K obtained by the free fit. 15 K can be regarded as an estimate of the uncertainty of  $T_g$  as the two alternative fits in this figure just meet the experimental data points, whose size (at least for those determined from our own spectra<sup>41</sup>) approximately corresponds to their uncertainty (about 10%). The same two alternative fit curves are also included in Supplementary Fig. 7a. None of the three VFT fits shown matches the experimental results on deeply supercooled water as measured, e.g., by Amann-Winkel *et al.* (stars)<sup>47</sup>. To be compatible with the low-temperature data, somewhere in the NML  $\tau(T)$  must start to deviate from the VFT behaviour derived from the high-temperature data. This means that there is an FST. Based on these pure-water data, we cannot say whether it is a sudden or a smeared-out change of slope. In the quenched 5 mol% LiCl solution (Fig. 2), the latter is found.

Data on extremely supercooled water may be criticised because the methods used to produce it could lead to different types of water, compared to water that hypothetically would be reached by slow supercooling if crystallization would not intervene<sup>48</sup>. However, we want to point out that the above conclusions on the inevitable occurrence of a FST can also be drawn when estimating the low-temperature behaviour of pure water by the extrapolation-based dashed line in Fig. 2.



**Supplementary Fig. 7 | Relaxation time of pure water above and below the NML. a**

Crosses and pluses: Arrhenius plot of  $\tau(T)$  above the NML, based on refs. 41 and 42, respectively, as also shown in Fig. 2 and Supplementary Fig. 6. The closed stars show additional data for deeply supercooled water below the NML from ref. 47. The lines are three alternative VFT fits [combining eqs. (1) and (6)] of the high-temperature data with free parameters and with  $T_g$  fixed to values that are 15 K lower or higher than 166 K (see legend). (The dash-dotted line is the same as the dash-dotted line in Fig. 2 and as the red solid line in Supplementary Fig. 6.) **b** Enlarged view of the high-temperature data, including the two fits with highest and lowest  $T_g$ .

## References

- <sup>1</sup> H. Vogel, *Phys. Z.* **22**, 645 (1921); G. S. Fulcher, *J. Am. Ceram. Soc.* **8**, 339 (1925); G. Tammann and W. Hesse, *Z. Anorg. Allg. Chem.* **156**, 245 (1926).
- <sup>2</sup> P. Lunkenheimer, S. Kastner, M. Köhler, and A. Loidl, *Phys. Rev. E* **81**, 051504 (2010).
- <sup>3</sup> P. Lunkenheimer and A. Loidl, in *The Scaling of Relaxation Processes*, edited by F. Kremer and A. Loidl (Springer, Cham, 2018), p. 23.
- <sup>4</sup> C. A. Angell, in *Relaxations in Complex Systems*, edited by K. L. Ngai and G. B. Wright (NRL, Washington, DC, 1985), p. 3.
- <sup>5</sup> J. C. Mauro, Y. Yueb, A. J. Ellisona, P. K. Gupta, and D. C. Allana, *PNAS* **106**, 19780 (2009).
- <sup>6</sup> J. Krausser, K. H. Samwer, and A. Zaccone, *PNAS* **112**, 13762 (2015).
- <sup>7</sup> R. Böhmer, K. L. Ngai, C. A. Angell, and D. J. Plazek, *J. Chem. Phys.* **99**, 4201 (1993).
- <sup>8</sup> D. J. Plazek and K. L. Ngai, *Macromolecules* **24**, 1222 (1991); R. Böhmer and C. A. Angell, *Phys. Rev. B* **45**, 10091 (1992).
- <sup>9</sup> L.-M. Wang, C. A. Angell, and R. Richert, *J. Chem. Phys.* **125**, 074505 (2006).
- <sup>10</sup> S. Emmert, M. Wolf, R. Gulich, S. Krohns, S. Kastner, P. Lunkenheimer, and A. Loidl, *Eur. Phys. J. B* **83**, 157 (2011).
- <sup>11</sup> P. Lunkenheimer, S. Krohns, S. Riegg, S. G. Ebbinghaus, A. Reller, and A. Loidl, *Eur. Phys. J. Special Topics* **180**, 61 (2010).
- <sup>12</sup> D. W. Davidson and R. H. Cole, *J. Chem. Phys.* **19**, 1484 (1951).
- <sup>13</sup> P. Lunkenheimer and A. Loidl, *Chem. Phys.* **284**, 205 (2002).
- <sup>14</sup> P. Lunkenheimer, M. Köhler, S. Kastner, and A. Loidl, in *Structural Glasses and Supercooled Liquids: Theory, Experiment, and Applications*, edited by P. G. Wolynes and V. Lubchenko (Wiley, Hoboken, NJ, 2012), chap. 3.
- <sup>15</sup> U. Schneider, R. Brand, P. Lunkenheimer, and A. Loidl, *Phys. Rev. Lett.* **84**, 5560 (2000).
- <sup>16</sup> K. S. Cole and R. H. Cole, *J. Chem. Phys.* **9**, 341 (1941).
- <sup>17</sup> S. Kastner, M. Köhler, Y. Goncharov, P. Lunkenheimer, and A. Loidl, *J. Non-Cryst. Solids* **357**, 510 (2011).
- <sup>18</sup> C. Monnin, M. Dubois, N. Papaiconomou, and J.-P. Simonin, *J. Chem. Eng. Data* **47**, 1331 (2002).
- <sup>19</sup> M.-Y. Li, L.-S. Wang, and J. Gmehling, *Ind. Eng. Chem. Res.* **50**, 3621 (2011).
- <sup>20</sup> C.-H. Yim and Y. A. Abu-Lebdeh, *J. Electrochem. Soc.* **165**, A547 (2018).
- <sup>21</sup> A. H. Narten, F. Vaslow, and H. A. Levy, *J. Chem. Phys.* **58**, 5017 (1973).
- <sup>22</sup> I. L. Green, A. R. Lacey, and M. G. Keats, *Chem. Phys. Lett.* **134**, 385 (1987).
- <sup>23</sup> M. Kobayashi and H. Tanaka, *Phys. Rev. Lett.* **106**, 125703 (2011).
- <sup>24</sup> M. Kobayashi and H. Tanaka, *J. Phys. Chem. B* **115**, 14077 (2011).
- <sup>25</sup> J. Dupuy, J. F. Jal, C. Ferradou, P. Chieux, A. F. Wright, R. Calemczuk, and C. A. Angell, *Nature* **296**, 138 (1982).
- <sup>26</sup> H. Kanno, *J. Phys. Chem.* **91**, 1967 (1987).
- <sup>27</sup> K. Hofer, A. Hallbrucker, E. Mayer, and G. P. Johari, *J. Chem. Phys.* **93**, 4674 (1989).
- <sup>28</sup> G. P. Johari, A. Hallbrucker, and E. Mayer, *Nature* **330**, 552 (1987).
- <sup>29</sup> C. T. Moynihan, A. J. Easteal, J. Wilder, and J. Tucker, *J. Phys. Chem.* **78**, 2673 (1974).
- <sup>30</sup> C. T. Moynihan, A. J. Easteal, J. Allam, M. A. DeBolt, and J. Tucker, *J. Am. Ceram. Soc.* **59**, 12 (1976).
- <sup>31</sup> J. L. Green, K. Ito, K. Xu, and C. A. Angell, *J. Phys. Chem. B* **103**, 3991 (1999).
- <sup>32</sup> C. T. Moynihan, *J. Am. Ceram. Soc.* **76**, 1081 (1993).
- <sup>33</sup> V. Velikov, S. Borick, and C. A. Angell, *J. Phys. Chem. B* **106**, 1069 (2002).
- <sup>34</sup> L.-M. Wang, V. Velikov, and C. A. Angell, *J. Chem. Phys.* **117**, 10184 (2002).
- <sup>35</sup> Y. Z. Yue, J. deC. Christiansen, and S. L. Jensen, *Chem. Phys. Lett.* **357**, 20 (2002).
- <sup>36</sup> Z. Chen, Z. Li, Y. Zhang, R. Liu, Y. Tian, and L.-M. Wang, *Eur. Phys. J. E* **37**, 52 (2014).
- <sup>37</sup> J. W. P. Schmelzer, *J. Chem. Phys.* **136**, 074512 (2012).
- <sup>38</sup> C. A. Angell, *Annu. Rev. Phys. Chem.* **55**, 559 (2004).
- <sup>39</sup> J. E. K. Schawe, *J. Chem. Phys.* **141**, 184905 (2014).
- <sup>40</sup> G. P. Johari, *J. Non-Cryst. Solids* **471**, 439 (2017).
- <sup>41</sup> P. Lunkenheimer, S. Emmert, R. Gulich, M. Köhler, M. Wolf, M. Schwab, and A. Loidl, *Phys. Rev. E* **96**, 062607 (2017).
- <sup>42</sup> D. Bertolini, M. Cassettari, and G. Salvetti, *J. Chem. Phys.* **76**, 3285 (1982).
- <sup>43</sup> U. Kaatze, *J. Chem. Eng. Data* **34**, 371 (1989).
- <sup>44</sup> R. Buchner, J. Bathel, and J. Stauber, *Chem. Phys. Lett.* **306**, 57 (1999).
- <sup>45</sup> C. Rønne, L. Thrane, P.-O. Åstrand, A. Wallqvist, K. V. Mikkelsen, and S. R. Keiding, *J. Chem. Phys.* **107**, 5319 (1997).
- <sup>46</sup> C. Rønne, P.-O. Åstrand, and S. R. Keiding, *Phys. Rev. Lett.* **82**, 2888 (1999).
- <sup>47</sup> K. Amann-Winkel et al., *Proc. Natl. Acad. Sci. USA* **110**, 17720 (2013).
- <sup>48</sup> S. Cerveny, F. Mallamace, J. Swenson, M. Vogel, and L. Xu, *Chem. Rev.* **116**, 7608 (2016).